AGU
ADVANCING EARTH AND SPACE SCIENCES

Geophysical Research Letters®

Key Points:

- Canopy-level evapotranspiration derived from thermal cameras agreed well with eddy covariance measurements
- Crown temperature measurements facilitated the estimation of individual-tree transpiration of co-occurring species using the same approach
- The results show interspecific differences in water use and response to drought that align with species traits

Correspondence to:

M. Javadian,
mostafa.javadian@nau.edu

Scaling Individual Tree Transpiration With Thermal Cameras Reveals Interspecies Differences to Drought Vulnerability

Mostafa Javadian[1] [ID], **Donald M. Aubrecht[2]**, **Joshua B. Fisher[3]**, **Russell L. Scott[4]** [ID], **Sean P. Burns[5,6]** [ID], **Jen L. Diehl[1,7]** [ID], **J. William Munger[8]** [ID], and **Andrew D. Richardson[1,7]** [ID]

[1]Center for Ecosystem Science and Society (ECOSS), Northern Arizona University, Flagstaff, AZ, USA, [2]Independent Researcher, Flagstaff, AZ, USA, [3]Schmid College of Science and Technology, Chapman University, Orange, CA, USA, [4]Southwest Watershed Research Center, USDA Agricultural Research Service, Tucson, AZ, USA, [5]Department of Geography, University of Colorado Boulder, Boulder, CO, USA, [6]NSF National Center for Atmospheric Research, Boulder, CO, USA, [7]School of Informatics, Computing, and Cyber Systems (SICCS), Northern Arizona University, Flagstaff, AZ, USA, [8]School of Engineering and Applied Sciences, Harvard University, Cambridge, MA, USA

Abstract Understanding tree transpiration variability is vital for assessing ecosystem water-use efficiency and forest health amid climate change, yet most landscape-level measurements do not differentiate individual trees. Using canopy temperature data from thermal cameras, we estimated the transpiration rates of individual trees at Harvard Forest and Niwot Ridge. PT-JPL model was used to derive latent heat flux from thermal images at the canopy-level, showing strong agreement with tower measurements ($R^2 = 0.70$–0.96 at Niwot, 0.59–0.78 at Harvard at half-hourly to monthly scales) and daily RMSE of 33.5 W/m^2 (Niwot) and 52.8 W/m^2 (Harvard). Tree-level analysis revealed species-specific responses to drought, with lodgepole pine exhibiting greater tolerance than Engelmann spruce at Niwot and red oak showing heightened resistance than red maple at Harvard. These findings show how ecophysiological differences between species result in varying responses to drought and demonstrate that these responses can be characterized by deriving transpiration from crown temperature measurements.

Plain Language Summary Understanding how forests use water, especially during droughts, is crucial for a changing climate. We developed a method using thermal cameras to estimate individual tree water loss (transpiration), something traditional methods lack. These cameras capture temperature data from the tree crown, which is then used to estimate transpiration rates. Tests in two forests showed this method aligns well with existing water use measurements. The study also revealed fascinating differences in how species handle drought. For instance, lodgepole pine outperformed Engelmann spruce in one forest, while red oak proved more resistant than red maple in the other. This shows that the thermal cameras can help assess how different trees resist drought conditions. This thermal camera technique has the potential to become a valuable tool for monitoring forest health as our climate evolves.

1. Introduction

Transpiration is the process of water movement through a plant, from the soil, through the stem and leaves, and out through stomata to the atmosphere, and its evaporation from aerial parts, such as leaves, stems, and flowers (Reddy, 2007). Tree transpiration represents an important component of total evapotranspiration in many terrestrial ecosystems and is crucial for understanding and managing ecosystem water resources (Peters et al., 2010). Accurate estimation of transpiration at the individual tree level is essential for understanding how trees respond to drought, ensuring the survival of key species, and developing sustainable forest management strategies that boost resistance to future climate change (Fisher et al., 2017).

While direct measurement of individual crown transpiration remains an elusive goal, each of the current methods used to estimate it present challenges at scale. For instance, sap flow sensors offer a valuable means to estimate transpiration at the individual tree level by directly measuring sap movement through the xylem and can provide crucial insights into water use patterns (Smith & Allen, 1996). However, issues like sensor calibration, scaling measurements to sapwood area, and spatial variability make it challenging to obtain precise measurements of tree transpiration (Granier & Loustau, 1994). Micrometeorological methods, such as the Bowen ratio technique and

eddy covariance, can be used to measure evapotranspiration of tree stands and forests with much better temporal resolution, but these methods cannot be used at the individual tree level (Baldocchi, 2003).

Transpiration is directly linked to the energy balance of vegetation (Gates, 1968). This relationship arises because the energy available to plants is partitioned into latent heat (LE, used in transpiration) and sensible heat (H, used in warming the surrounding air) (Bonan, 2019). By constraining the energy balance through precise measurements and modeling of these energy fluxes, we can estimate transpiration rates (Bonan, 2019). This approach leverages the principle that the sum of LE and H, along with vegetation heat flux, must equal the net radiation received by the plant canopy (Jones, 1985). One solution to estimate transpiration through leaf energy balance is to use thermal imaging for the forest canopy temperature or the temperature of individual tree crowns. Thermal imaging can be used to measure canopy temperatures with high spatiotemporal frequency at scales ranging from experimental plots (Javadian et al., 2023), flux tower footprints (Javadian, Scott, et al., 2024; Still et al., 2022), drones (Javadian et al., 2022; Still et al., 2019), to satellites (Fisher et al., 2020). Although thermal imaging has been extensively used to enhance our understanding of ecosystem structure and function, it has not yet been utilized to estimate tree-level transpiration.

Several models have been proposed to estimate transpiration using canopy temperature obtained from thermal imaging. The Priestley-Taylor Jet Propulsion Laboratory model (PT-JPL model, Fisher et al., 2008), has been extensively used to estimate transpiration due to its reduced requirement for local measurements. PT-JPL is used in NASA's ECOsystem Spaceborne Thermal Radiometer Experiment on Space Station (ECOSTRESS) evapotranspiration product and demonstrated high agreement with tower measurements (Fisher et al., 2020). However, the ECOSTRESS 70-m spatial resolution and 3–5 days temporal resolution is not adequate to capture transpiration at the tree level nor frequent enough to capture faster tree responses to variations in weather conditions. By contrast, continuous thermal imaging at the site level, like at an eddy covariance tower, can advance our understanding of the PT-JPL model and, consequently, tree transpiration (Farella et al., 2022).

In this study, we use high-resolution near-surface thermal imagery from two distinct forest ecosystems, including an evergreen subalpine conifer forest (Niwot Ridge) and a deciduous temperate forest (Harvard Forest) to estimate transpiration rates of individual trees, and their responses to drought. First, we employ the PT-JPL model to estimate canopy ET and validate our estimates against tower-based measurements. Subsequently, we apply the model to individual tree crowns across various species to examine the differences in tree-level modeled transpiration in response to drought across timescales ranging from diurnal to seasonal. Finally, we interpret the variations in modeled transpiration among different species in terms of their ecophysiological differences.

2. Materials and Methods

2.1. Site Descriptions

Our first field site is the 26 m tall Ameriflux "US-NR1" tower (40.0329°N 105.5464°W) at the University of Colorado's Mountain Research Station on Niwot Ridge, 40 km west of Boulder, CO. The tower is surrounded by a mix of evergreen needleleaf species: lodgepole pine (*Pinus contorta* Douglas ex Loudon), Engelmann spruce (*Picea engelmannii* Parry ex Engelm.), and subalpine fir (*Abies lasiocarpa* (Hook.) Nutt.). Lodgepole pine and Engelmann spruce exhibit distinct adaptations to drought and shade. Lodgepole pine, tolerating a wider moisture range, thrives in both sun and moderate drought (Amman, 1978). Conversely, Engelmann spruce flourishes in cool, high-elevation moisture, but stresses during prolonged dryness (Anderson, 1956). Additionally, lodgepole pine is typically deeper rooted (Despain, 2001), and Engelmann spruce is shallow-rooting at high-elevations (Robert, 1990). Shade tolerance further distinguishes them: Engelmann spruce thrives beneath the canopy, while lodgepole pine prefers full sun for optimal growth (Keane et al., 2018). Bowling et al. (2018) showed winter transpiration at Niwot is close to zero for both species.

We mounted an A655sc thermal camera (FLIR Systems, Inc., 640 × 480 pixel resolution, 45° FOV) near the top of the US-NR1 tower. The camera points east, is inclined about 30° below the horizon to reduce the effects of direct sunlight and have a view across the canopy, and collects images continuously every 5 min. Mounted atop the same tower, observing the same canopy are: two VIS-NIR networked digital cameras (StarDot NetCam SC), a 4-channel net radiometer (Kipp & Zonen CNR4), and a dual temperature/relative humidity probe (Vaisala HMP35c). These instruments provide measurements necessary for correcting interference in the images recorded by the FLIR cameras and for interpreting differences between canopy and air temperature. More details about the

sites and cameras are in Aubrecht et al. (2016). The US-NR1 tower provided 30 min LE, sensible heat flux (H), incoming shortwave radiation (SW_IN), outgoing shortwave radiation (SW_OUT), incoming longwave radiation (LW_IN), net radiation (R_n), friction velocity (u*), air temperature (T_a), relative humidity (RH), and vapor pressure deficit (VPD) data that were used in the current analysis (Burns et al., 2015). At US-NR1, air temperature and humidity sensors were mounted at 2, 8, and 21.5 m heights but we used 21.5 m level to represent our top of canopy region of interest (ROI).

Our second field site is the 40 m tall "Barn Tower" (42.5353°N 72.1899°W) at the Harvard Forest, 110 km west of Boston, MA. The tower is surrounded by mixed forest stands dominated by red oak (*Quercus rubra* L.), red maple (*Acer rubrum* L.), and white pine (*Pinus strobus* L.). Shallow root systems render red maple more vulnerable to drought events when compared to red oaks (Abbott, 1974). The latter possess deeper root structures, granting them access to subterranean water reserves. Red maple also exhibits moderate shade tolerance, flourishing in partially shaded environments (Abbott, 1974). Red oak, on the other hand, demonstrates a preference for full sun exposure (Auchmoody & Clay, 1979).

We mounted an A655sc thermal camera (FLIR Systems, Inc., 640 × 480 pixel resolution, 45° FOV) atop the Barn tower. The camera points north, is inclined 20–30° below the horizon to reduce the effects of direct sunlight and have a view across the canopy, and collects images continuously every 15 min. Supporting measurements including a digital camera, a 4-channel net radiometer, and a dual temperature/relative humidity probe are made similar to the Niwot instrumentation. We also used 30 min LE, H, and u* data of US-Ha1 (Urbanski et al., 2007). The US-Ha1 tower is situated approximately 2 km from the thermal camera location on the Barn tower. A comparison of ECOSTRESS land surface temperature (LST) data at 70-m resolution, acquired between 2018 and 2023, revealed a high degree of similarity between the Barn and US-Ha1 (Figure S1 in Supporting Information S1). The mean instantaneous LST (2018–2023) for the Barn was only 0.37 ± 0.82°C higher than US-Ha1 ($R^2 = 0.93$), indicating minimal LST differentials across these regions. Although no eddy flux measurements were taken at the Barn tower, the high degree of LST similarity suggests that LE, H, and u* are likely comparable between the two sites; nevertheless, radiation components, air temperature, and humidity data were acquired through the instrumentation on the Barn tower (Richardson & Aubrecht, 2024). At Barn tower, those sensors were mounted at the location of thermal camera which was above the canopies.

Both US-NR1 and Barn towers were equipped with PhenoCam cameras, facilitating the capturing of RGB images at these sites. These images were used for selection of ROIs and monitoring of the growing season (Seyednasrollah et al., 2019). Thermal and Visible images of the canopy at Harvard and Niwot are provided in Figure 1 with ROIs delineated for each species to enable individual tree analysis. The ROIs were carefully defined to ensure they remain fully vegetated throughout the entire growing season, based on RGB imagery. Additionally, Figures S2 and S3 in Supporting Information S1 present the canopy temperatures along with the differences between canopy and air temperatures for the trees highlighted.

The Standardized Precipitation Evapotranspiration Index (SPEI) (Vicente-Serrano et al., 2010) was used for drought assessment in this study. SPEI is a modified version of the Standardized Precipitation Index (SPI) (McKee et al., 1993) and considers both potential evapotranspiration and precipitation. Here we used SPEI_12, as a 12-month SPEI, obtained from (http://sac.csic.es/spei/map/maps.html) with a one-degree spatial resolution and a monthly time resolution.

2.2. Model to Estimate Transpiration

The tree transpiration (T) model used in this study is the transpiration component obtained from the PT-JPL algorithm (Fisher et al., 2008), which has been widely validated throughout the literature as one of the top-performing global remote sensing ET models (e.g., Chen et al., 2014; Fisher et al., 2020; Purdy et al., 2018). PT-JPL retrieves actual ET by reducing potential ET (ET_p) starting with the PT equation (Fisher et al., 2011; Priestley & Taylor, 1972):

$$ET_p = \alpha \frac{\Delta}{\Delta + \gamma} R_n$$
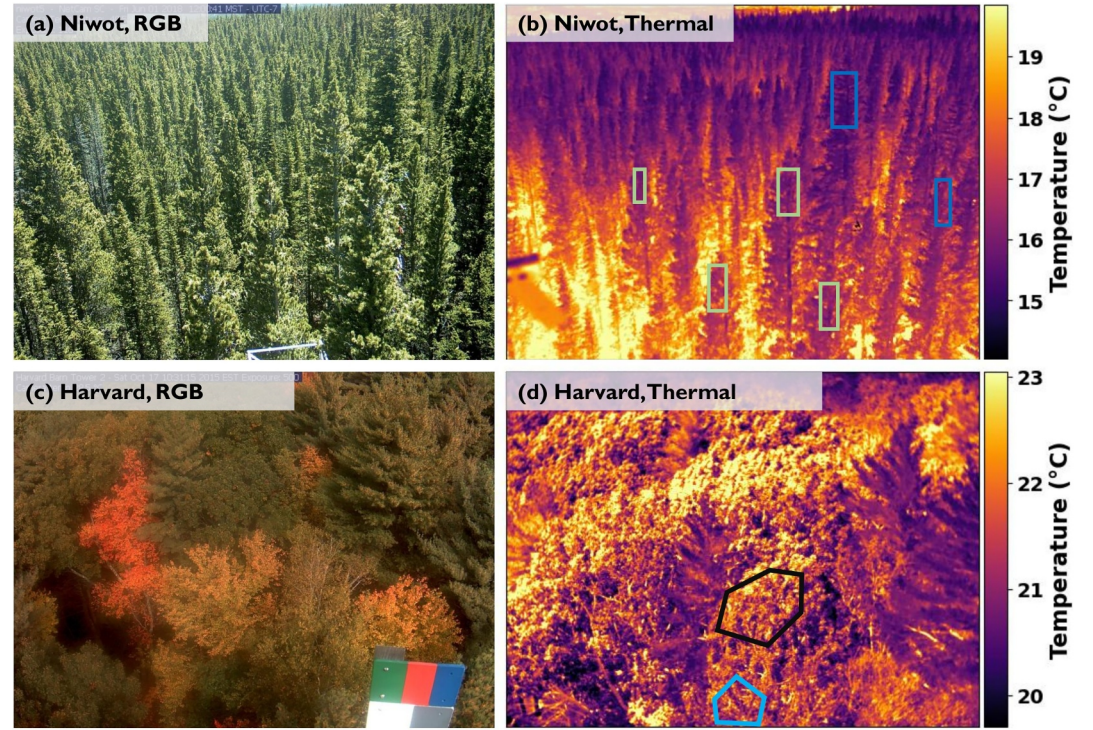
Figure 1. Example from a single temporal acquisition of RGB and the thermal camera in (a) and (b): US-NR1 showing ROIs with light green rectangles for lodgepole pine and dark blue rectangles for Engelmann spruce on 1st June 2018, at 12:00 (UTC-7), (c and d): Harvard Forest Barn tower showing ROIs with black polygon for red oak and light blue polygons for red maple on 17th October 2015, at 10:31 (UTC-5).

where Δ is the slope of the saturation-to-vapor pressure curve, dependent on near-surface air temperature, (T_a; °C) and water vapor pressure (e_a; kPa), γ is the psychrometric constant (0.066 kPa/°C), and α is the PT coefficient of 1.26 (unitless); ET_p is in units of Wm^{-2}.

A series of ecophysiological scalar functions (unitless; 0–1), based on atmospheric vapor pressure deficit (Da; kPa), RH (fraction), and vegetation indices, including normalized difference and soil adjusted vegetation indices (NDVI obtained from MODIS and SAVI; unitless), simultaneously reduce ET_p to actual ET, and partition total ET into three sources for canopy transpiration (ET_c), soil evaporation (ET_s), and interception evaporation (ET_i) that has been described in Fisher et al. (2008, 2020):

$$ET = ET_c + ET_s + ET_i$$

$$ET_c = (1 - f_{wet}) f_g f_T f_M \alpha \frac{\Delta}{\Delta + \gamma} R_{nc}$$

$$ET_s = (f_{wet} + f_{SM}(1 - f_{wet})) \alpha \frac{\Delta}{\Delta + \gamma} (R_{ns} - G)$$

$$ET_i = f_{wet} \alpha \frac{\Delta}{\Delta + \gamma} R_{nc}$$

$$f_T = e^{-\left(\frac{T_a - T_{opt}}{T_{opt}}\right)^2}$$

where f_{wet} is relative surface wetness (RH^4), f_g is green canopy fraction (f_{APAR}/f_{IPAR}), f_T is a plant temperature constraint, f_M is a plant moisture constraint ($f_{APAR}/f_{APARmax}$), and f_{SM} is a soil moisture constraint (RH^{D_a}). f_{APAR} is absorbed photosynthetically active radiation (PAR), f_{IPAR} is intercepted PAR, T_{opt} (°C) is the optimum

temperature linked to plant phenology and G is the soil heat flux (Wm^{-2}). R_{nc} and R_{ns} are R_n for the canopy and the soil, respectively, based on leaf area index derived from NDVI.

At the canopy-level analysis (entire field of view), we compare the total ET (ET$_c$ + ET$_s$ + ET$_i$) of PT-JPL model with the total ET measured by the flux tower. At tree-level analysis, we focus solely on the transpiration (ET$_c$) of the trees from PT-JPL since ET$_s$ and ET$_i$ are the same for the trees. The code utilized in this study is primarily derived from Purdy (2020) (https://github.com/sciencebyAJ/PTJPL-1D), with specific adaptations made to facilitate canopy temperature based ET at the tree-level.

The outgoing longwave radiation (LW$_{out}$) in R_n (i.e., canopy R_n) was calculated using the corrected canopy temperature data from thermal cameras via Stefan-Boltzmann equation:

$$LW_{out} = \varepsilon \sigma T_c{}^4$$

where LW$_{out}$ is the upward longwave radiation from the canopy surface (Wm^{-2}), ε is the emissivity (unitless) derived from previous studies (Aubrecht et al., 2016), σ is the Stefan-Boltzmann constant (=5.67×10^{-8} Wm^{-2} K^{-4}), and T_c is the average canopy temperature of all canopies at the field of view for the canopy-level analysis and the average canopy temperature of the associated ROI of the individual trees for the tree-level analysis. T_c has been corrected for background and atmospheric impacts based on Aubrecht et al. (2016).

3. Results

The results for predicted LE based on our model versus measured LE show good agreement at both sites (Figure 2). The coefficient of determination, R^2, for Niwot, assessed at half-hourly, daily, and monthly intervals, stands at 0.70, 0.77, and 0.96, respectively. Meanwhile, for Harvard, the corresponding values are 0.62, 0.78, and 0.59 respectively; The Root Mean Square Error (RMSE) for Niwot is 12.9 Wm^{-2}/month whereas for Harvard it is 53.5 Wm^{-2}/month. The model overestimated LE in higher R_n and underestimated LE in lower R_n at both sites.

At Niwot, the differences in transpiration between lodgepole pine and Engelmann spruce showed a strong response to drought conditions (Figures 3a–3c). Notably, the peaks in their transpiration differences coincided significantly with the zenith of the SPEI_12, where more negative SPEI values indicate heightened drought severity. Specifically, during the summers of 2017 and 2018, characterized by prominent drought conditions, the transpiration differences reached their peaks with higher transpiration in lodgepole pine than Engelmann spruce. A threshold SPEI value of approximately −1 was identified as the point at which more pronounced changes in transpiration occurred (Figure 3c). This suggests that when water availability declines past this threshold, plants exhibit a stronger physiological response, likely due to increased drought stress. Conversely, in the absence of significant drought stress during the summer of 2016 and spring of 2019, the transpiration differences between the two species were negligible. This implies that lodgepole pine was the more drought-tolerant species, and Engelmann spruce was the more drought-sensitive species. However, this distinction is influenced by a range of factors, including physiological traits such as root depth, stomatal behavior, and other adaptive responses, which should be considered.

To further explore the species differences, the diurnal transpiration patterns revealed that lodgepole pine consistently exhibited higher transpiration rates than Engelmann spruce throughout most daylight hours in all months (Figure S4 in Supporting Information S1). This difference was most pronounced around midday. Notably, April, marking the typical onset of the growing season at Niwot, demonstrated the greatest mid-day transpiration differences between the two species compared to other months.

Similarly in Harvard, the variations in transpiration rates between red maple and red oak exhibited significant sensitivity to drought conditions (Figures 3d–3f). Over the period from the drought-free summer of 2014 to the prolonged drought of the summer of 2016, the transpiration dynamics between red maple and red oak underwent a noteworthy shift. Initially, in 2014, red maple demonstrated higher transpiration rates compared to red oak. However, by 2016, during the drought period, red maple experienced a decline in transpiration, leading to lower rates than those observed in red oak. This implies red maple was the more drought-sensitive species, and red oak was the more drought-tolerant species.
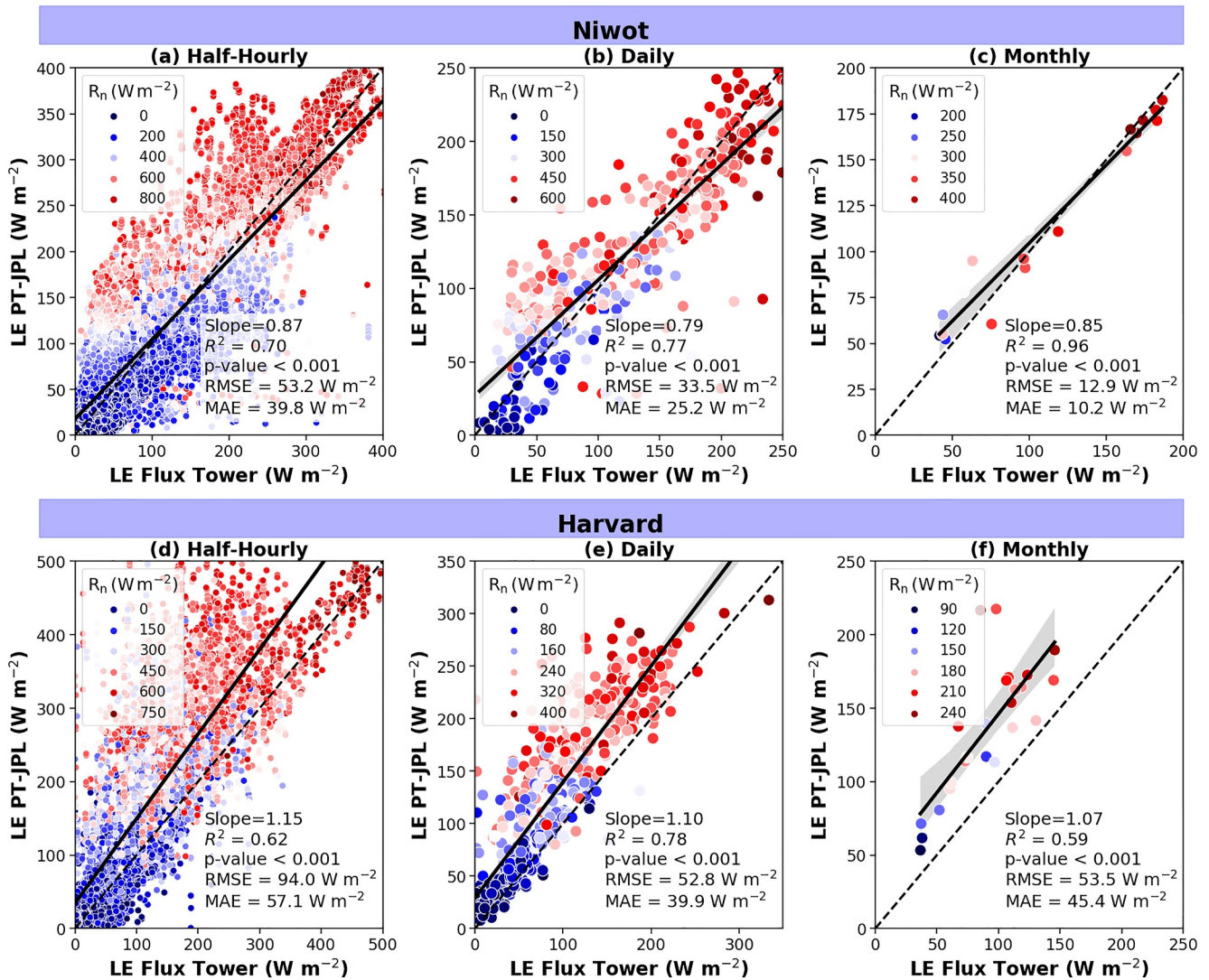
Figure 2. PT-JPL exhibits robust skill in estimating daytime LE of growing seasons. Each scatterplot represents LE estimates by PT-JPL versus in situ LE measurements at the flux tower in half-hourly, daily, and monthly scales. The 1:1 and linear regression lines are shown by the dashed and solid black lines, respectively. The PT-JPL LE represents the entire canopy level LE within each site.

The diurnal transpiration patterns of red oak and red maple exhibited a marked similarity to their respective drought responses (Figure S5 in Supporting Information S1). Throughout most of the afternoon, when soil moisture is more constrained than in the morning, red oak demonstrated higher transpiration rates compared to red maple, particularly during the months of June, July, and August. Conversely, during the morning, when soil moisture limitations are less pronounced, red maple exhibited higher transpiration rates than red oak.

4. Discussion

We used the PT-JPL model to estimate canopy-level LE using thermal cameras and we validated our findings against eddy covariance measurements. The results demonstrated a strong agreement between PT-JPL canopy-level thermal camera-based LE and eddy flux LE during daytime throughout the growing season at both study sites. This approach was also applied to estimate individual tree transpiration among co-occurring species. The results revealed interspecific differences in water use and drought response that corresponded with known traits of each species.
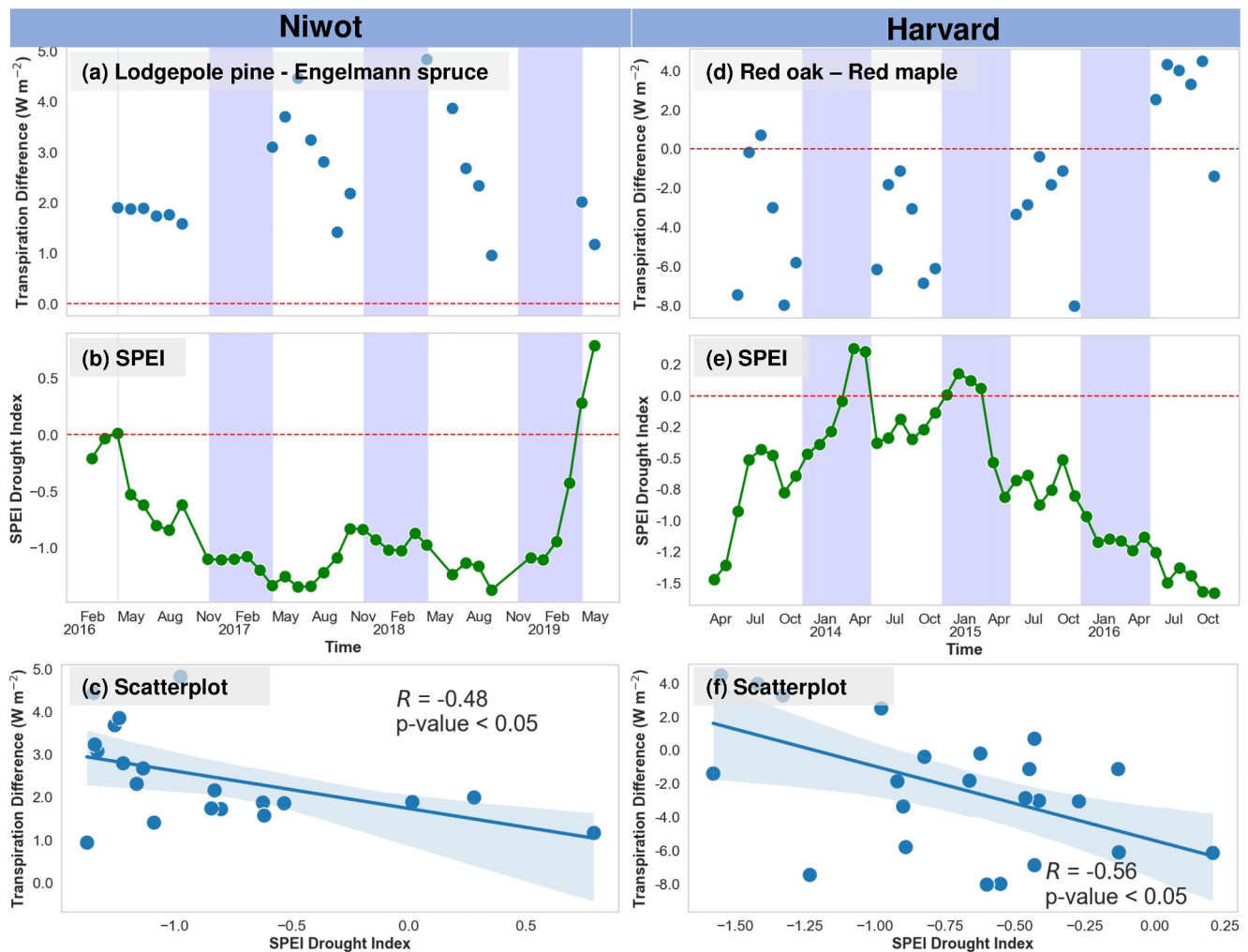
Figure 3. (a) The average mid-day monthly transpiration difference between Lodgepole pine and Engelmann spruce at Niwot Ridge, (b) SPEI drought index, (c) Scatterplot between the average mid-day monthly transpiration difference between Lodgepole pine and Engelmann spruce and SPEI drought index in US-NR1, (d) The average mid-day monthly transpiration difference between red oak and red maple at Harvard Forest, (e) SPEI drought index, (f) Scatterplot between the average mid-day monthly transpiration difference between red oak and red maple and SPEI drought index at Harvard Forest. The blue-shaded regions represent the canopy dormancy. The red dotted lines indicate the $y = 0$ line.

4.1. PT-JPL Performance

Thermal camera-based LE from PT-JPL showed good performance against eddy flux LE. Still, we observed a tendency for LE overestimation under conditions of higher R_n and underestimation under lower R_n across sub-daily, daily, and monthly scales (Figure S6 in Supporting Information S1). This phenomenon can be attributed to our thermal camera measurements being mainly directed toward the upper canopy, which typically exhibits higher canopy temperatures and greater transpiration rates. Consequently, during periods of elevated R_n (e.g., midday in summer), it is unsurprising that model estimations for upper canopy transpiration exceed the average footprint of the tower. Conversely, during times of reduced R_n (e.g., early morning in fall), upper canopy temperatures may be cooler relative to the lower canopy, resulting in lower LE values for the upper canopy compared to the entire flux tower footprint, while also potentially overlooking the effects of diffuse radiation in the sub-canopy and shading from leaves. This is supported by the differences between PT-JPL upper and lower canopy estimation of LE in Niwot where upper canopy ROIs exhibited higher LE during the summer compared to lower canopy ROIs, while the reverse trend was observed in winter (Figure S7 in Supporting Information S1). The overall bias at Niwot, however, was minimal; but, the estimate was biased high at Harvard, possibly due to the need to increase the sensitivity of one of the ecophysiological constraint functions within PT-JPL at this site such

as soil moisture constraint (f_{SM}). In the PT-JPL, f_{SM} is traditionally estimated by RH. However, García et al. (2013) enhanced f_{SM} by incorporating the thermal inertia concept, utilizing soil temperature and albedo, which significantly improved their model performance. Implementing a similar approach could represent a key area of improvement for the LE estimates at Harvard. The overestimation of PT-JPL ET in the higher R_n and cloudy days was also reported by other studies. For example, Liu et al. (2021) revealed an overestimation of instantaneous and daily PT-JPL ET in a humid temperate forest ecosystem, due to misrepresenting local climatic conditions, poor upscaling of instantaneous measurement to the daily scale on cloudy days, and inadequately characterizing surface vegetation index similar to the overestimation that Wu et al. (2022) found during the summer over 15 cropland flux sites in North America.

4.2. Utilizing Thermal Cameras to Estimate Individual Tree Transpiration

Thermal cameras have been employed extensively in studying canopy temperature across diverse tree species and plant functional types in various ecosystems. However, our study marks the pioneering utilization of thermal cameras to estimate individual tree transpiration rates. Our method demonstrated promising efficacy and offers a potential alternative to traditional invasive techniques like sap flow sensors. Several advantages of employing thermal cameras over other methods for estimating individual tree transpiration rates are evident. First, thermal cameras enable the comparison of individual tree transpiration rates among neighboring trees utilizing the same images with differing regions of interest. By contrast, the utilization of sap flow sensors, necessitates sensor biases corrections and scaling to whole tree levels based on assumptions about xylem transport variability, rendering accurate computation of tree transpiration rates challenging but they may perform better than thermal cameras in areas where the species density or viewing geometry precludes clear ROIs for individual species. Second, canopy temperature data obtained from thermal cameras can be directly integrated into various evapotranspiration models grounded in energy balance principles, facilitating the estimation of different components of ecosystem evapotranspiration. Third, thermal cameras can easily be deployed at flux towers and provides an independent estimate of transpiration to complement flux tower LE measurements and assist with gap-filling.

4.3. Comparison of Individual Tree Transpiration Responses to Drought

At both sites, intraspecific differences in transpiration responses to drought align with species traits (Figure 3 and Figure S8 in Supporting Information S1). Our findings from Niwot revealed that lodgepole pine exhibits greater drought tolerance compared to Engelmann spruce. This finding is supported by Danyagri et al. (2023) and Justin DeRose (2023) that found that lodgepole pine have several adaptations that help them survive drought, such as efficient water use and deep root systems. The sap flow measurements at Niwot from Hu et al. (2010) showed lodgepole pine having the highest transpiration rates, followed by Engelmann spruce and then fir. Horton (1958) observed that lodgepole pine in Alberta can develop deep roots extending up to 4 feet. Conversely, Kaufmann (1975) suggest the majority of Engelmann spruce roots are within the top 30–46 cm of soil, rendering them vulnerable to surface disturbances and drought conditions, particularly in shallow soil environments. Additionally, the diurnal transpiration patterns showed that lodgepole pine consistently demonstrated higher transpiration rates compared to Engelmann spruce during most daylight hours across all months, with a peak around midday. This difference may be attributed to the species' rooting strategies, which the shallow roots of Engelmann spruce are more susceptible to midday soil evaporation, whereas the deeper roots of lodgepole pine are less affected (Despain, 2001; Robert, 1990) in addition to higher stomatal conductance in lodgepole pine (Kaufmann, 1982).

Similarly, at Harvard, we found red oak was more tolerant to drought than red maple. While Barton and Gleeson (1996) suggested that red maple might be more drought tolerant than red oak, most evidence points in the other direction. For example, aligned with our finding, Matheny et al. (2017) showed, during a soil dry down, transpiration and stem water storage decreased by more than 80% and 28% in red maples but only by 31% and 1% in red oaks in Michigan. Additionally, Fekedulegn et al. (2003) demonstrated that red oak outperform red maple, chestnut oak, and yellow-poplar in terms of drought resilience in West Virginia. Furthermore, the topographic positions occupied by the two species are different. Although they can coexist in various forest settings, red oak demonstrates a greater affinity for well-drained sites, such as rocky ridges and uplands (Green et al., 2010). Conversely, red maple thrives along the fringes of swamps and wetlands, indicating a lower tolerance for drought conditions (Alexander & Arthur, 2010; Stein & Acciavatti, 2001). Additionally, throughout most of the afternoon, when soil moisture is more constrained than in the morning, red oak demonstrated higher transpiration rates

compared to red maple. This could be due to red oak's deeper rooting system, which better accesses limited moisture compared to the shallower roots of red maple (Abbott, 1974), thicker leaves, and smaller stomata (Fekedulegn et al., 2003).

4.4. Limitations and Future Directions

The study was constrained by the use of uniform RH, T_a, and NDVI values for all ROIs at each site, as these variables were only available for the entire site footprint. This approach may not fully account for variability among neighboring trees, which can differ due to distinct ecophysiological traits of each species. Additionally, while LST at the Barn and US-Ha1 towers were similar, potential differences in LE between the Barn and US-Ha1 towers are still expected but it could not be assessed due to the unavailability of LE data for the Barn tower.

5. Conclusions

Our study highlights the power of thermal imaging combined with the PT-JPL model to estimate individual tree transpiration and assess species-specific responses to drought stress. This capability is critical for understanding the dynamic nature of water use in forest ecosystems, particularly in the face of a changing climate. By resolving ET at the tree level, we can gain deeper insights into ecosystem resilience at the tree-level. Notably, our findings revealed significant differences in drought tolerance between co-occurring species using thermal cameras at both study sites. Lodgepole pine at Niwot and red oak at Harvard displayed a greater ability to maintain transpiration rates during drought compared to Engelmann spruce and red maple, respectively. This underlines the importance of considering species composition when evaluating ecosystem vulnerability to climate change. Furthermore, the good agreement between thermal imagery-derived ET and tower flux measurements at daily and monthly scales validates the PT-JPL potential for large-scale applications, though there remains room for further improvement. This study revealed how leveraging crown temperature measurements through ET modeling can opens doors for non-invasive monitoring of drought stress at the individual tree level.

Data Availability Statement

Thermal data has been archived at figshare (Javadian, Aubrecht, & Richardson, 2024). Flux tower data can be accessed through the AmeriFlux data portal (https://ameriflux.lbl.gov). PhenoCam data is available at https://phenocam.nau.edu/webcam/roi/niwot5/EN_1000/ and https://phenocam.nau.edu/webcam/roi/harvardbarn2/DB_1000/. Barn tower data is provided by Richardson and Aubrecht (2024). SPEI data can be found at http://sac.csic.es/spei/map/maps.html. ECOSTRESS LST and MODIS NDVI data are accessible via https://search.earthdata.nasa.gov/.

References

Abbott, H. G. (1974). Some characteristics of fruitfulness and seed germination in red maple. *Tree Planters' Notes*, 25(2), 25–27.

Alexander, H. D., & Arthur, M. A. (2010). Implications of a predicted shift from upland oaks to red maple on forest hydrology and nutrient availability. *Canadian Journal of Forest Research*, 40(4), 716–726. https://doi.org/10.1139/x10-029

Amman, G. D. (1978). Biology, ecology, and causes of outbreaks of the mountain pine beetle in lodgepole pine forests. In *Symposium on theory and practice of mountain pine beetle management in Lodgepole pine forests* (pp. 39–53).

Anderson, I. V. (1956). Engelmann spruce, its properties and uses. USDA Forest Service, Issue. I. F. a. R. E. Station.

Aubrecht, D. M., Helliker, B. R., Goulden, M. L., Roberts, D. A., Still, C. J., & Richardson, A. D. (2016). Continuous, long-term, high-frequency thermal imaging of vegetation: Uncertainties and recommended best practices. *Agricultural and Forest Meteorology*, 228–229, 315–326. https://doi.org/10.1016/j.agrformet.2016.07.017

Auchmoody, L. R. S., & Clay, H. (1979). *Oak soil-site relationships in northwestern West Virginia*. U.S. Department of Agriculture, Forest Service, Northeastern Forest Experiment Station.

Baldocchi, D. D. (2003). Assessing the eddy covariance technique for evaluating carbon dioxide exchange rates of ecosystems: Past, present and future. *Global Change Biology*, 9(4), 479–492. https://doi.org/10.1046/j.1365-2486.2003.00629.x

Barton, A. M., & Gleeson, S. K. (1996). Ecophysiology of seedlings of oaks and red maple across a topographic gradient in eastern Kentucky. *Forest Science*, 42(3), 335–342. https://doi.org/10.1093/forestscience/42.3.335

Bonan, G. (2019). Leaf temperature and energy fluxes. In *Climate change and terrestrial ecosystem modeling* (pp. 152–166). Cambridge University Press. https://doi.org/10.1017/9781107339217.011

Bowling, D. R., Logan, B. A., Hufkens, K., Aubrecht, D. M., Richardson, A. D., Burns, S. P., et al. (2018). Limitations to winter and spring photosynthesis of a Rocky Mountain subalpine forest. *Agricultural and Forest Meteorology*, 252, 241–255. https://doi.org/10.1016/j.agrformet.2018.01.025

Burns, S. P., Blanken, P. D., Turnipseed, A. A., Hu, J., & Monson, R. K. (2015). The influence of warm-season precipitation on the diel cycle of the surface energy balance and carbon dioxide at a Colorado subalpine forest site. *Biogeosciences*, 12(23), 7349–7377. https://doi.org/10.5194/bg-12-7349-2015

Chen, Y., Xia, J., Liang, S., Feng, J., Fisher, J. B., Li, X., et al. (2014). Comparison of satellite-based evapotranspiration models over terrestrial ecosystems in China. *Remote Sensing of Environment*, *140*, 279–293. https://doi.org/10.1016/j.rse.2013.08.045

Danyagri, G., Baral, S. K., Waterhouse, M. J., & Newsome, T. A. (2023). Climate-mediated lodgepole pine tree growth response to thinning and fertilization in interior British Columbia. *Forest Ecology and Management*, *544*, 121161. https://doi.org/10.1016/j.foreco.2023.121161

Despain, D. G. (2001). Dispersal ecology of lodgepole pine (*Pinus contorta* Dougl.) in its native environment as related to Swedish forestry. *Forest Ecology and Management*, *141*(1), 59–68. https://doi.org/10.1016/S0378-1127(00)00489-8

Farella, M. M., Fisher, J. B., Jiao, W., Key, K. B., & Barnes, M. L. (2022). Thermal remote sensing for plant ecology from leaf to globe. *Journal of Ecology*, *110*(9), 1996–2014. https://doi.org/10.1111/1365-2745.13957

Fekedulegn, D., Hicks, R. R., & Colbert, J. J. (2003). Influence of topographic aspect, precipitation and drought on radial growth of four major tree species in an Appalachian watershed. *Forest Ecology and Management*, *177*(1), 409–425. https://doi.org/10.1016/S0378-1127(02)00446-2

Fisher, J. B., Lee, B., Purdy, A. J., Halverson, G. H., Dohlen, M. B., Cawse-Nicholson, K., et al. (2020). ECOSTRESS: NASA's next generation mission to measure evapotranspiration from the international space station. *Water Resources Research*, *56*(4), e2019WR026058. https://doi.org/10.1029/2019wr026058

Fisher, J. B., Melton, F., Middleton, E., Hain, C., Anderson, M., Allen, R., et al. (2017). The future of evapotranspiration: Global requirements for ecosystem functioning, carbon and climate feedbacks, agricultural management, and water resources. *Water Resources Research*, *53*(4), 2618–2626. https://doi.org/10.1002/2016WR020175

Fisher, J. B., Tu, K. P., & Baldocchi, D. D. (2008). Global estimates of the land–atmosphere water flux based on monthly AVHRR and ISLSCP-II data, validated at 16 FLUXNET sites. *Remote Sensing of Environment*, *112*(3), 901–919. https://doi.org/10.1016/j.rse.2007.06.025

Fisher, J. B., Whittaker, R. J., & Malhi, Y. (2011). ET come home: Potential evapotranspiration in geographical ecology. *Global Ecology and Biogeography*, *20*(1), 1–18. https://doi.org/10.1111/j.1466-8238.2010.00578.x

García, M., Sandholt, I., Ceccato, P., Ridler, M., Mougin, E., Kergoat, L., et al. (2013). Actual evapotranspiration in drylands derived from in-situ and satellite data: Assessing biophysical constraints. *Remote Sensing of Environment*, *131*, 103–118. https://doi.org/10.1016/j.rse.2012.12.016

Gates, D. M. (1968). Transpiration and leaf temperature. *Annual Review of Plant Physiology*, *19*(1), 211–238. https://doi.org/10.1146/annurev.pp.19.060168.001235

Granier, A., & Loustau, D. (1994). Measuring and modelling the transpiration of a maritime pine canopy from sap-flow data. *Agricultural and Forest Meteorology*, *71*(1), 61–81. https://doi.org/10.1016/0168-1923(94)90100-7

Green, S. R., Arthur, M. A., & Blankenship, B. A. (2010). Oak and red maple seedling survival and growth following periodic prescribed fire on xeric ridgetops on the Cumberland Plateau. *Forest Ecology and Management*, *259*(12), 2256–2266. https://doi.org/10.1016/j.foreco.2010.02.026

Horton (1958). *Rooting habits of lodgepole pine*. F. R. Division.

Hu, J., Moore, D. J. P., Riveros-Iregui, D. A., Burns, S. P., & Monson, R. K. (2010). Modeling whole-tree carbon assimilation rate using observed transpiration rates and needle sugar carbon isotope ratios. *New Phytologist*, *185*(4), 1000–1015. https://doi.org/10.1111/j.1469-8137.2009.03154.x

Javadian, M., Aubrecht, D., & Richardson, A. (2024). Canopy temperature data at Niwot Ridge and Harvard Forest [Dataset]. *Figshare*. https://doi.org/10.6084/m9.figshare.26319217

Javadian, M., Scott, R. L., Biederman, J. A., Zhang, F., Fisher, J. B., Reed, S. C., et al. (2023). Thermography captures the differential sensitivity of dryland functional types to changes in rainfall event timing and magnitude. *New Phytologist*, *240*(1), 114–126. https://doi.org/10.1111/nph.19127

Javadian, M., Scott, R. L., Woodgate, W., Richardson, A. D., Dannenberg, M. P., & Smith, W. K. (2024). Canopy temperature dynamics are closely aligned with ecosystem water availability across a water- to energy-limited gradient. *Agricultural and Forest Meteorology*, *357*, 110206. https://doi.org/10.1016/j.agrformet.2024.110206

Javadian, M., Smith, W. K., Lee, K., Knowles, J. F., Scott, R. L., Fisher, J. B., et al. (2022). Canopy temperature is regulated by ecosystem structural traits and captures the ecohydrologic dynamics of a semiarid mixed conifer forest site. *Journal of Geophysical Research: Biogeosciences*, *127*(2), e2021JG006617. https://doi.org/10.1029/2021JG006617

Jones, M. B. (1985). Chapter 3—Plant microclimate. In J. Coombs, D. O. Hall, S. P. Long, & J. M. O. Scurlock (Eds.), *Techniques in bioproductivity and photosynthesis* (2nd ed., pp. 26–40). Pergamon. https://doi.org/10.1016/B978-0-08-031999-5.50013-3

Justin DeRose, R. (2023). Conserving lodgepole pine genetic diversity in the face of uncertainty. *Forest Ecology and Management*, *545*, 121235. https://doi.org/10.1016/j.foreco.2023.121235

Kaufmann, M. R. (1975). Leaf water stress in Engelmann spruce: Influence of the root and shoot environments 1. *Plant Physiology*, *56*(6), 841–844. https://doi.org/10.1104/pp.56.6.841

Kaufmann, M. R. (1982). Leaf conductance as a function of photosynthetic photon flux density and absolute humidity difference from leaf to air. *Plant Physiology*, *69*(5), 1018–1022. https://doi.org/10.1104/pp.69.5.1018

Keane, R. E., Mahalovich, M. F., Bollenbacher, B. L., Manning, M. E., Loehman, R. A., Jain, T. B., et al. (2018). Effects of climate change on forest vegetation in the northern Rockies. In J. E. Halofsky, & D. L. Peterson (Eds.), *Climate change and rocky mountain ecosystems* (pp. 59–95). Springer International Publishing. https://doi.org/10.1007/978-3-319-56928-4_5

Liu, N., Oishi, A. C., Miniat, C. F., & Bolstad, P. (2021). An evaluation of ECOSTRESS products of a temperate montane humid forest in a complex terrain environment. *Remote Sensing of Environment*, *265*, 112662. https://doi.org/10.1016/j.rse.2021.112662

Matheny, A. M., Fiorella, R. P., Bohrer, G., Poulsen, C. J., Morin, T. H., Wunderlich, A., et al. (2017). Contrasting strategies of hydraulic control in two codominant temperate tree species. *Ecohydrology*, *10*(3), e1815. https://doi.org/10.1002/eco.1815

McKee, T. B., Doesken, N. J., & Kleist, J. (1993). The relationship of drought frequency and duration to time scales. In *Proceedings of the 8th conference on applied climatology*.

Peters, E. B., McFadden, J. P., & Montgomery, R. A. (2010). Biological and environmental controls on tree transpiration in a suburban landscape. *Journal of Geophysical Research*, *115*(G4), G04006. https://doi.org/10.1029/2009JG001266

Priestley, C. H. B., & Taylor, R. J. (1972). On the assessment of surface heat flux and evaporation using large-scale parameters. *Monthly Weather Review*, *100*(2), 81–92. https://doi.org/10.1175/1520-0493(1972)100<0081:OTAOSH>2.3.CO;2

Purdy, A. J. (2020). PT-JPL 1D: A one-dimensional implementation of the Priestley-Taylor Jet Propulsion Laboratory model. [Source Code]. https://github.com/sciencebyAJ/PTJPL-1D

Purdy, A. J., Fisher, J. B., Goulden, M. L., Colliander, A., Halverson, G., Tu, K., & Famiglietti, J. S. (2018). SMAP soil moisture improves global evapotranspiration. *Remote Sensing of Environment*, *219*, 1–14. https://doi.org/10.1016/j.rse.2018.09.023

Reddy, S. M. (2007). *University Botany-III: (Plant taxonomy, plant embryology, plant physiology)*. New Age International.

Richardson, A. D., & Aubrecht, D. (2024). Radiometric and meteorological data from Harvard Forest Barn Tower 2011-2017 ver 7 [Dataset]. *Environmental Data Initiative*. https://doi.org/10.6073/pasta/763bb2443c8e15ba88e6a895cf44b381

Robert, A. R. (1990). Engelmann spruce (*Picea engelmannii*). In *Silvics of North America: Volume 1, conifers*. U.S. Department of Agriculture, Forest Service, Southern Research Station. Retrieved from https://srs.fs.usda.gov/pubs/misc/ag_654/volume_1/picea/engelmannii.htm

Seyednasrollah, B., Young, A. M., Hufkens, K., Milliman, T., Friedl, M. A., Frolking, S., et al. (2019). *PhenoCam Dataset v2.0: Vegetation phenology from digital camera imagery, 2000-2018*. ORNL Distributed Active Archive Center.

Smith, D. M., & Allen, S. J. (1996). Measurement of sap flow in plant stems. *Journal of Experimental Botany*, *47*(12), 1833–1844. https://doi.org/10.1093/jxb/47.12.1833

Stein, J. B. D., & Acciavatti, R. (2001). *Field guide to native oak species in eastern North America* (Vol. FHTET-03-01). USDA Forest Service, Forest Health Technology Enterprise Team.

Still, C., Powell, R., Aubrecht, D., Kim, Y., Helliker, B., Roberts, D., et al. (2019). Thermal imaging in plant and ecosystem ecology: Applications and challenges. *Ecosphere*, *10*(6), e02768. https://doi.org/10.1002/ecs2.2768

Still, C. J., Page, G., Rastogi, B., Griffith, D. M., Aubrecht, D. M., Kim, Y., et al. (2022). No evidence of canopy-scale leaf thermoregulation to cool leaves below air temperature across a range of forest ecosystems. *Proceedings of the National Academy of Sciences of the United States of America*, *119*(38), e2205682119. https://doi.org/10.1073/pnas.2205682119

Urbanski, S., Barford, C., Wofsy, S., Kucharik, C., Pyle, E., Budney, J., et al. (2007). Factors controlling CO_2 exchange on timescales from hourly to decadal at Harvard Forest. *Journal of Geophysical Research*, *112*(G2), G02020. https://doi.org/10.1029/2006JG000293

Vicente-Serrano, S. M., Beguería, S., & López-Moreno, J. I. (2010). A multiscalar drought index sensitive to global warming: The standardized precipitation evapotranspiration index. *Journal of Climate*, *23*(7), 1696–1718. https://doi.org/10.1175/2009JCLI2909.1

Wu, J., Feng, Y., Liang, L., He, X., & Zeng, Z. (2022). Assessing evapotranspiration observed from ECOSTRESS using flux measurements in agroecosystems. *Agricultural Water Management*, *269*, 107706. https://doi.org/10.1016/j.agwat.2022.107706